

Signature of cloud-base height skewness in ARM microwave water radiometer data: Implications for cloud radiative parameterizations in GCMs

Christopher A. Jeffery^a and Anthony B. Davis^a

^aLos Alamos National Laboratory (NIS-2), PO Box 1663, Mail Stop C-323,
Los Alamos, NM 87545, USA

ABSTRACT

The statistics of ground-based retrievals of cloud liquid water path using the microwave water radiometer (MWR) are typically assumed to be independent of the cloud's absolute position in the column. Furthermore, translational invariance implies statistical parity, i.e. invariance under reflection, of cloud-base height (z_{bot}) and cloud-top height distributions. This symmetry is necessarily broken, especially under conditions of high boundary-layer relative humidity for which a minimum large-scale lifting condensation level leads to the generation of a significant positive skewness in the distribution function of z_{bot} . We suggest that the signature of this boundary effect is visible in ARM MWR time-series collected at the TWP site. Motivated by the MWR analysis, we incorporate a minimum lifting condensation level into the analytic model of unresolved low-cloud optical variability developed by Jeffery & Austin (*J. Atmos. Sci.*, to appear). Preliminary results indicate that the effect of cloud-base height skewness on mean oceanic low-cloud reflectivity averaged over GCM spatial scales (order 100 km) is significant.

Keywords: Cloud-base height skewness, ARM, MWR, statistical cloud scheme, cloud optical parameterization

1. INTRODUCTION

Numerous studies have established that the determination of average cloud reflectivity, \bar{R} , using only the first moment of shortwave (SW) optical depth, $\bar{\tau}_{\text{SW}}$, via the approximation, $\bar{R} = R(\bar{\tau}_{\text{SW}})$, systematically underestimates \bar{R}^{1-5} . This systematic underestimation results from the convexity of $R(\tau)$ and is called the plane-parallel homogeneous (PPH) bias. Of course, the PPH approximation is avoidable if the in-cloud probability distribution function of τ_{SW} , $P_{\tau_{\text{SW}}}$, is known. Then, by definition, $\bar{R} = \int R(\xi) P_{\tau_{\text{SW}}}(\xi) d\xi$. The PPH approximation also leads to biases in the determination of cloud longwave (LW) optical properties⁶.

Observational studies of low-cloud P_{τ} generally find a nearly Gaussian distribution when the variance of τ , σ_{τ}^2 , is relatively small and exponential—or possibly log-normal—tails when σ_{τ}^2 is relatively large^{4,7-10}. This general behaviour was explained by Considine et al.¹¹ who showed that a normal distribution of cloud thickness combined with a linear low-cloud liquid water density profile leads to a distribution of longwave optical depth, $P_{\tau_{\text{LW}}}$, with tails ranging from Gaussian to exponential. An extension of the Considine model for τ_{SW} exhibits a similar behaviour¹². Wood and Taylor¹³ related fluctuations in longwave optical depth, τ_{LW} , at fixed cloud-top height, z_{top} , to fluctuations in potential temperature, θ , and total water, q_t . Thus normal distributions of θ and q_t at constant z_{top} are broadly consistent with observational distributions of τ_{LW} with Gaussian-to-exponential tails. Jeffery and Austin¹⁴ considered both τ_{LW} and τ_{SW} and demonstrated that values of the P_{τ} width parameter $\nu_{\text{SW}} \equiv (\bar{\tau}_{\text{SW}}/\sigma_{\tau})^2$ and cloud fraction, A_c , compiled by Barker et al.⁷ from Landsat data are consistent with a normal distribution of variability that includes cloud-top height fluctuations, z'_{top} .

In the work of Considine et al.¹¹ and Jeffery and Austin¹⁴ the pdf of cloud-base height, z_{bot} , is not explicitly considered. As we shall see in Sect. 4 the z_{bot} -skewness, $\zeta_{z_{\text{bot}}}$, in these models is, implicitly, ≤ 0 when the

Further author information: (Send correspondence to C.A.J.)

C.A.J.: E-mail: cjeffery@lanl.gov, Telephone: 1 505 665 9169

A.B.D.: E-mail: adavis@lanl.gov, Telephone: 1 505 665 6577

underlying distributions of θ and q_t are symmetric. Moreover, $\zeta_{z_{\text{bot}}}$ in the Wood and Taylor¹³ model is, explicitly, ≤ 0 although the authors restrict their analysis to the case where $A_c = 1$ and $\zeta_{z_{\text{bot}}} = 0$. In contrast, in-situ and surface-based measurements of z_{bot} distributions of low-clouds often indicate a positive skewness^{15–17}. In this article we suggest a simple mechanism for the creation of positive skewness in z_{bot} , namely, the thermodynamic boundary condition $z_{\text{bot}} \geq 0$ where the reference height $z = 0$ is a large-scale minimum lifting condensation level. We show that under conditions of high boundary-layer relative humidity, symmetric distributions of θ and q_t result in $\zeta_{z_{\text{bot}}} > 0$. This breaks the statistical parity, i.e. symmetry by reflection, between z_{bot} and z_{top} fluctuations implied by the Considine et al.¹¹ model.

This article is organized as follows. In Sect. 2 we analyze the relationship between $\nu \equiv (\bar{\tau}/\sigma_\tau)^2$ and A_c in both 45 Landsat images and 6 years of daily ARM microwave water radiometer data and find evidence of relatively large ν that are not explained by translationally invariant models with symmetric underlying distributions^{11,13,14}. The Jeffery-Austin model of low-cloud optical statistics is briefly derived in Sect. 3.1, and the boundary-condition $z_{\text{bot}} \geq 0$ is then incorporated into the model in Sect. 3.2. In Sect. 4 a new parameter β_c is introduced that is a measure of the influence of the constraint $z_{\text{bot}} \geq 0$, and in Sect. 5 the β_c -dependence of ν - A_c relations is explored. The impact of β_c on mean in-cloud SW reflectivity is briefly investigated in Sect. 6, and Sect. 7 contains a summary.

2. MOTIVATION

We begin by considering the relationship between $\nu \equiv (\bar{\tau}/\sigma_\tau)^2$ and A_c first analyzed by Barker et al.⁷. Barker et al. retrieved ν_{SW} and A_c from 45 Landsat images and suggested that ν_{SW} is a monotonic function of A_c . This suggestion found theoretical support by Jeffery and Austin¹⁴ who derived the following expressions for $\overline{\tau_{\text{SW}}^p}$ and A_c :

$$\overline{\tau_{\text{SW}}^p} \sim A_c^{-1} \int_{-\infty}^{S_0 + \Gamma_w z_{\text{top}}} (S_0 + \Gamma_w z_{\text{top}} - \xi)^{5p/3} P_{s_*}(\xi) d\xi, \quad (1)$$

$$A_c = \int_{-\infty}^{S_0 + \Gamma_w z_{\text{top}}} P_{s_*}(\xi) d\xi, \quad (2)$$

where S_0 is the mean water density surplus or deficit, Γ_w is the liquid water density lapse rate and s_* represents fluctuations in θ , q_t and z_{top} . These equations are derived and discussed in detail in Sect. 3.1. For our purposes here, the key feature of Eqs. (1) and (2) is that they predict a 1-to-1 mapping between ν_{SW} and A_c for a given P_{s_*} .

Although a theoretical calculation of P_{s_*} is not available at this time, a reasonable estimation is a stretched exponential distribution of the form

$$P_{s_*} = c_1 \exp(-c_2 |s_*|^\alpha), \quad (3)$$

where $1 \leq \alpha \leq 2$ and the constants c_1 and c_2 are set by the normalization $\int P_{s_*}(\xi) d\xi = 1$ and $\int \xi^2 P_{s_*}(\xi) d\xi = \sigma_{s_*}^2$. Note that for $\alpha = 2$ P_{s_*} is Gaussian while the choice $\alpha = 1$ gives an exponential distribution. A Gaussian distribution of unresolved variability was assumed in the pioneering work of Sommeria and Deardorff¹⁸ and Mellor¹⁹ and an exponential distribution by Bougeault²⁰.

A comparison of ν_{SW} vs A_c predicted by Eqs. (1–3) for $\alpha \in \{2, 5/3, 4/3, 1\}$ and $\nu_{\text{SW}} \leq 3$ is shown in Fig. 1. Also shown is Landsat data from Table 2 in Barker et al.⁷. The figure reveals that broadening the distribution of s_* , i.e. $\alpha \downarrow$, decreases ν_{SW} for a given A_c in the range $A_c < 0.95$. Overall the envelop of the present model with $1 \leq \alpha \leq 2$ does a good job of explaining most of Barker et al.⁷'s data in the range $\nu_{\text{SW}} \leq 3$. The notable exception, however, are a number of scenes (5–7) with values of ν_{SW} that are significantly larger than the prediction of the present model. A possible explanation is an exceedingly narrow P_{s_*} , i.e. $\alpha > 2$, but this is unlikely since distributions of tracers, e.g. θ and q_t , in turbulent velocity fields have pdfs that are Gaussian or broader.

Further evidence of relatively large values of ν for a given A_c is present in ground-based microwave radiometer (MWR) measurements of cloud liquid water path, i.e. τ_{LW} , at the DOE ARM Tropical Western Pacific (TWP)

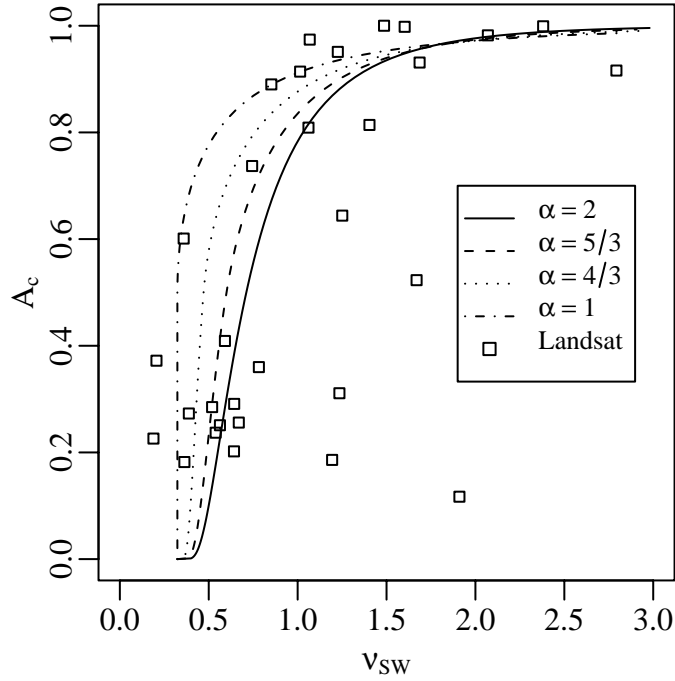


Figure 1. Comparison of ν_{SW} vs A_c for $\nu_{\text{SW}} \leq 3$. Lines are from Eqs. (1–3) with $\alpha \in \{2, 5/3, 4/3, 1\}$. Landsat data is from Table 2 in Barker et al.⁷. The present model does not capture the very large values ν_{SW} found in some Landsat scenes.

Manus site. This ARM data product consists of typically 24 hours of measurements at an interval of 20 seconds (about 4000 measurements per file). Assuming a constant sweep of around 5 m s^{-1} each data file represents a 400-500 km segment of τ_{LW} measurements at a spatial resolution of 100-200 meters. A comparison of ν_{LW} vs A_c calculated from MWR measurements is shown in Fig. 2. The data encompasses the period 1996-2002, and scenes where the liquid water path exceeds $0.16 \text{ cm} \approx 1600 \text{ g m}^{-2}$ are excluded to limit contamination by multi-layer clouds. A threshold of $0.003 \text{ cm} \approx 30 \text{ g m}^{-2}$ is used in this analysis. A comparison of the Landsat and MWR data in figures 1 and 2, respectively, reveals that the MWR data exhibits greater scatter. This is not unexpected since a single Landsat scene contains over 4 million pixels whereas a MWR data segment contains roughly 4000 measurements.

The present model of Jeffery and Austin¹⁴ differentiates between SW scattering and LW absorption. The LW analog of Eq. (1) is¹⁴

$$\overline{\tau_{\text{LW}}^p} \sim A_c^{-1} \int_{-\infty}^{S_0 + \Gamma_w z_{\text{top}}} (S_0 + \Gamma_w z_{\text{top}} - \xi)^{2p} P_{s_*}(\xi) d\xi. \quad (4)$$

Note that the only difference between Eqs. (1) and (4) is the exponent of the integrand²¹. The predictions of Eqs. (2–4) are also shown in Fig. 2 for $\alpha \in \{2, 5/3, 4/3, 1\}$. As in Fig. 1, the envelope of the present model captures the relatively smaller values of ν_{LW} quite well but larger values are not well explained. However, it should be emphasized that the MWR data segments also contain a diurnal signal which could potentially impact the observed ν - A_c relationship. An analysis of the effect of the diurnal cycle on single-layer cloud statistics is beyond the scope of the present investigation.

In the following sections a model of single-layer cloud optical statistics is developed that accounts for the

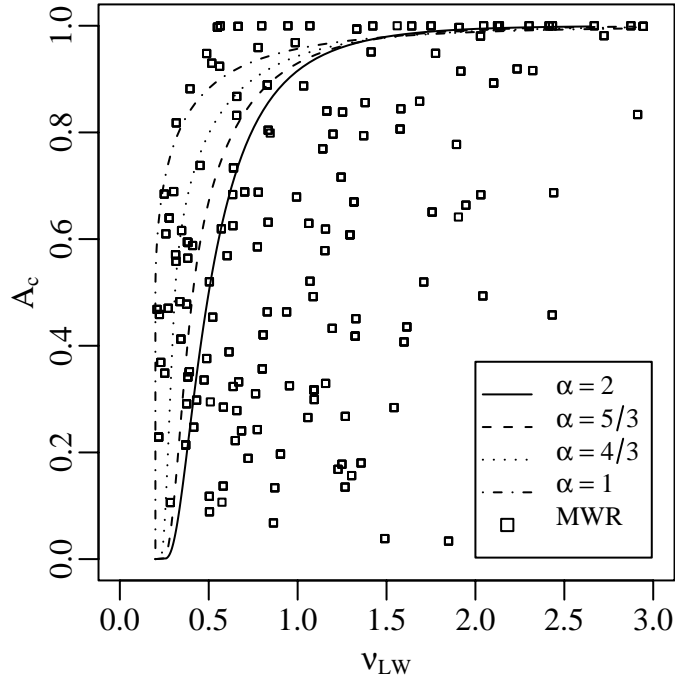


Figure 2. Comparison of ν_{LW} vs A_c for $\nu_{\text{SW}} \leq 3$. Lines are from Eqs. (2–4) with $\alpha \in \{2, 5/3, 4/3, 1\}$. MWR data is from the ARM TWP site. As per Fig. 1, relatively large values of ν_{LW} are not captured by the present model.

relatively low values of ν found in Landsat and MWR data.

3. MODEL DERIVATIONS

3.1. Derivation of the Jeffery–Austin Model

We begin this section with a derivation of the model of low-cloud optical statistics developed by Jeffery and Austin¹⁴ [See also Eqs. (1–4)]. Consider a single-layer cloud field. As in Jeffery and Austin¹⁴ we itemize these important assumptions: (i) horizontal variability of the cloud field exceeds vertical variability and (ii) cloud liquid water increases linearly with height above cloud base. Our notation is as follows. The variable dependence (x) labels unresolved horizontal variability, whereas (z) indicates a vertical dependence which by assumption (i) is essentially non-stochastic, i.e. vertical fluctuations are assumed negligible.

Consider the Sommeria-Deardorff-Mellor statistical cloud scheme^{18,19} for cloud liquid water density, q_l , combined with assumption (i):

$$q_l(x, z) = a_L \{S(z) - s(x)\}_H, \quad (5)$$

where S is the mean water density surplus ($S > 0$) or deficit ($S < 0$), $s(x)$ represents horizontal fluctuations in θ and q_t , $a_L < 1$ is a parameter that accounts for condensational latent-heat release and $\{A\}_H : \{A < 0\}_H = 0, \{A \geq 0\}_H = A$ is a Heaviside bracket. Furthermore, using assumption (ii) we have $S(z) = S_0 + \Gamma_w z$ where $z = 0$ is an arbitrary reference height in the boundary layer, e.g. the surface.

Using Eq. (5) we evaluate the integral of $q_l^p(x, z)$ from cloud base $z_{\text{bot}}(x)$ to cloud top $z_{\text{top}}(x) = z_{\text{top}} + z'_{\text{top}}(x)$:

$$\int_{z_{\text{bot}}(x)}^{z_{\text{top}}(x)} q_l^p(x, z) dz = \frac{a_L^p \Gamma_w^{-1}}{p+1} \{S_0 + \Gamma_w z_{\text{top}} - s_*(x)\}_H^{p+1}, \quad (6)$$

where

$$s_*(x) = s(x) - \Gamma_w z'_{\text{top}}(x), \quad (7)$$

and we have used $z_{\text{bot}} = \Gamma_w^{-1}(-S_0 + s)$ from (ii). Note that Eq. (7) for s_* includes fluctuations in z_{top} while the approach of Wood and Taylor¹³ assumes $z'_{\text{top}} = 0$.

Formulation of the shortwave and longwave optical depths follows from Eq. (6) given the appropriate functional relation $\tau \sim \int \text{func}(q_l, \dots) dz$. At this point, it is convenient to introduce the cloud thickness $h(x) = z_{\text{top}}(x) - z_{\text{bot}}(x)$ so that Eq. (6) is simply

$$\int_{z_{\text{bot}}(x)}^{z_{\text{top}}(x)} q_l^p(x, z) dz = \frac{(a_L \Gamma_w)^p}{p+1} h^{p+1}(x).$$

Following Considine et al.¹¹, τ_{LW} is strictly given by the “ h^2 model”

$$\tau_{\text{LW}}(x) \sim \frac{a_L}{2\Gamma_w} \{S_0 + \Gamma_w z_{\text{top}} - s_*(x)\}_H^2, \quad (8)$$

while the “ $h^{5/3}$ model” is more appropriate for τ_{SW} ^{14,21}:

$$\tau_{\text{SW}}(x) \sim \frac{3a_L^{2/3}}{5\Gamma_w} \{S_0 + \Gamma_w z_{\text{top}} - s_*(x)\}_H^{5/3}. \quad (9)$$

Eqs. (1), (2) and (4) follow immediately from Eqs. (8–9).

3.2. A New Formulation

In the derivation of τ in the previous subsection we did not consider the effect of a large-scale minimum lifting condensation level. As a result we were able to combine z_{bot} and z_{top} fluctuations into a single stochastic parameter s_* which represents h -fluctuations. Without loss of generality, let the reference height $z = 0$ be a large-scale minimum lifting condensation level. Then a new thermodynamic boundary condition appears: $z_{\text{bot}}(x) \geq 0$. Since we did not enforce $z_{\text{bot}}(x) \geq 0$ in Sec. 3.1, an implicit assumption used in the derivation of Eqs. (8–9) is $q_l(x, z = 0) = 0$. Below we derive new expressions for τ where $q_l(x, z = 0)$ may be greater than zero.

Returning to Eq. (6) we formulate $z_{\text{bot}}(x)$ according to

$$z_{\text{bot}}(x) = \Gamma_w^{-1} \{-S_0 + s(x)\}_H$$

which includes a Heaviside bracket that was not used in the derivation of Eq. (6). Using Eq. (5) and assumption (ii) we find

$$\int_{z_{\text{bot}}(x)}^{z_{\text{top}}(x)} q_l^p(x, z) dz = \frac{a_L^p \Gamma_w^{-1}}{p+1} [\{S_0 + \Gamma_w z_{\text{top}} - s_*(x)\}_H^{p+1} - \{S_0 - s(x)\}_H^{p+1}] \quad (10)$$

which includes a new term. The second term on the rhs of Eq. (10) is proportional to $q_l^p(x, z = 0)$ and reflects the impact of the boundary condition $z_{\text{bot}} \geq 0$ on τ . The new model formulations of τ follow immediately from Eq. (10):

$$\tau_{\text{LW}}(x) \sim \frac{a_L}{2\Gamma_w} [\{S_0 + \Gamma_w z_{\text{top}} - s_*(x)\}_H^2 - \{S_0 - s(x)\}_H^2], \quad (11)$$

$$\tau_{\text{SW}}(x) \sim \frac{3a_L^{2/3}}{5\Gamma_w} [\{S_0 + \Gamma_w z_{\text{top}} - s_*(x)\}_H^{5/3} - \{S_0 - s(x)\}_H^{5/3}]. \quad (12)$$

Evaluation of Eq. (11) or (12) depends critically on the correlation $\langle s_* s \rangle$. Here we consider two limiting cases:

Model NOZTOP: $z'_{\text{top}} = 0$ and therefore $s_* = s$.

Model DECORR: $\langle s_* s \rangle = 0$.

Model NOZTOP assumes $z'_{\text{top}} = 0$ which is an assumption also used in Wood and Taylor¹³. Model DECORR has a somewhat subtler interpretation. In this limiting case we assume that z'_{bot} and z'_{top} are comparable in magnitude and strongly correlated. Thus we have that

$$\langle s_* s \rangle \sim \langle (z'_{\text{top}} - z'_{\text{bot}}) z'_{\text{bot}} \rangle \approx 0.$$

Stated another way we assume that h and z_{bot} are uncorrelated and $\langle h^2 \rangle \neq 0$. Model DECORR further implies $\langle s^2 \rangle > \langle s_*^2 \rangle$.

In the Jeffery-Austin model, NOZTOP and DECORR with Gaussian P_s predict a correlation coefficient, ρ , between below-cloud boundary-layer humidity, RH, and in-cloud optical depth that potentially brackets the observational values. In particular ρ is approximately > 0.9 for NOZTOP and $\rho = 0$ for DECORR. In comparison, Klein et al.²² found a correlation coefficient $\rho = -0.5$ between A_c and boundary-layer temperature using monthly averages which is consistent with a τ -RH correlation in the range $0 < \rho < 1$.

4. MODEL EVALUATION

The second term on the rhs of Eqs. (11–12) represents the impact of the boundary condition $z_{\text{bot}} \geq 0$ on τ and is absent in the Jeffery-Austin model (i.e. Eqs. (8–9)). A useful dimensionless parameter, β_c , may be defined that reflects the relative contribution of this new term:

$$\beta_c \equiv \frac{\text{fraction}\{(S_0 - s > 0) \cap (\tau > 0)\}}{\text{fraction}\{\tau > 0\}} \equiv \frac{\text{fraction}\{q_l(z = 0) > 0\}}{A_c},$$

where $0 \leq \beta_c < 1$. Thus β_c represents the relative occurrence of cloud, i.e. $q_l > 0$, reaching the minimum lifting condensation level $z = 0$. Note that the value of β_c is equivalent for both τ_{SW} and τ_{LW} .

The parameter β_c can be evaluated for models NOZTOP and DECORR:

$$\beta_c^{\text{NOZTOP}} = \frac{\int_{-\infty}^{S_0} P_s(\xi) d\xi}{\int_{-\infty}^{S_0 + \Gamma_w z_{\text{top}}} P_s(\xi) d\xi}, \quad (13)$$

$$\beta_c^{\text{DECORR}} = \frac{\int_{-\infty}^{S_0 + \Gamma_w z_{\text{top}}} P_{s_*}(\xi) d\xi \int_{-\Gamma_w z_{\text{top}} + \xi}^{S_0} P_s(\xi_2) d\xi_2}{\int_{-\infty}^{S_0 + \Gamma_w z_{\text{top}}} P_{s_*}(\xi) d\xi \int_{-\Gamma_w z_{\text{top}} + \xi}^{\infty} P_s(\xi_2) d\xi_2}. \quad (14)$$

We can see from Eqs. (13–14) that $\beta_c \rightarrow 0$ as $S_0 \rightarrow -\infty$ for both models while $\beta_c \rightarrow 1$ as $z_{\text{top}} \rightarrow 0$ for NOZTOP and $\beta_c \rightarrow 1$ as $S_0 \rightarrow \infty$ for DECORR. The limit $\beta_c \rightarrow 1$ is, therefore, physically interesting.

Before discussing the relationship between β_c and $\zeta_{z_{\text{bot}}}$ it is useful to contrast $\zeta_{z_{\text{bot}}}(\beta_c = 0)$ for models NOZTOP and DECORR when P_s is symmetric. For model NOZTOP

$$\overline{z_{\text{bot}}^p}(\beta_c \rightarrow 0) = \lim_{S_0 \rightarrow -\infty} A_c^{-1} \int_{S_0}^{S_0 + \Gamma_w z_{\text{top}}} \Gamma_w^{-1}(-S_0 + \xi)^p P_s(\xi) d\xi. \quad (15)$$

Considering $p \in \{1, 2, 3\}$, it is clear from Eq. (15) that $\zeta_{z_{\text{bot}}} \leq 0$ for model NOZTOP when P_s is symmetric. For the case ($\beta_c = 0, A_c = 1$) considered by Wood and Taylor¹³, we have the special case $\zeta_{z_{\text{bot}}} = 0$. In contrast for model DECORR

$$\overline{z_{\text{bot}}^p}(\beta_c \rightarrow 0) = \lim_{S_0 \rightarrow -\infty} A_c^{-1} \int_{-\infty}^{S_0 + \Gamma_w z_{\text{top}}} P_{s_*}(\xi) d\xi \int_{S_0}^{\infty} \Gamma_w^{-1}(-S_0 + \xi_2)^p P_s(\xi_2) d\xi_2 \quad (16)$$

so that $\zeta_{z_{\text{bot}}}(\beta_c = 0) = 0$ for DECORR and symmetric P_s independent of A_c . Thus we find that the Jeffery-Austin model of cloud optical statistics in which z_{bot} is not treated explicitly allows for a range of $\zeta_{z_{\text{bot}}}$ that

depends on the assumed relationship between s and s_* . For the two models considered here, i.e. NOZTOP and DECORR, $\zeta_{z_{\text{bot}}} \leq 0$ when P_s is symmetric.

A comparison of $\zeta_{z_{\text{bot}}}(\beta_c)$ for models NOZTOP and DECORR is shown in Fig. 3 for $A_c \in \{0.3, 0.75, 0.95\}$ and Gaussian P_s and P_{s_*} . As expected, increasing β_c increases $\zeta_{z_{\text{bot}}}$ for both models. However, model NOZTOP exhibits a greater A_c -dependence. As per the discussion above, this behaviour is also expected since $\zeta_{z_{\text{bot}}}(\beta_c = 0)$ is A_c -dependent for NOZTOP but not DECORR.

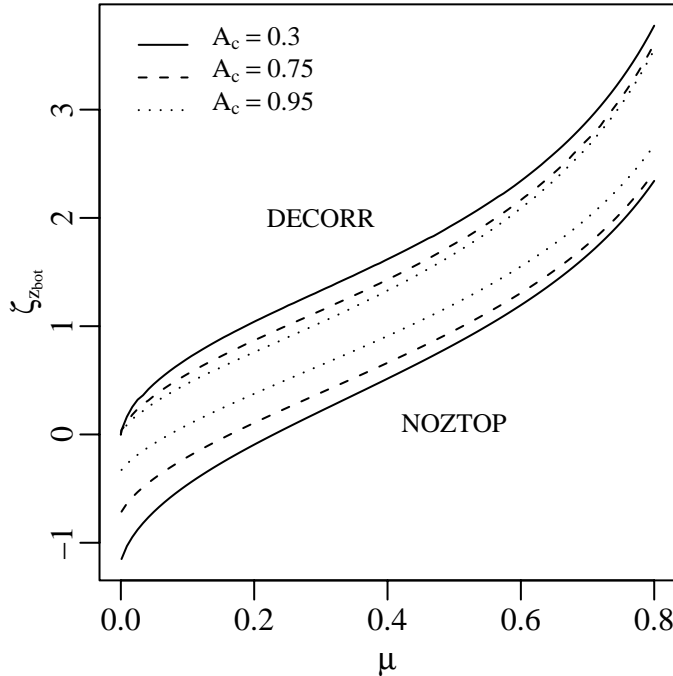


Figure 3. Comparison of $\zeta_{z_{\text{bot}}}$ for models NOZTOP and DECORR for $A_c \in \{0.3, 0.75, 0.95\}$ and Gaussian P_s and P_{s_*} . Skewness is calculated from Eqs. (15–16) and the definition $\zeta_{z_{\text{bot}}} \equiv \overline{z_{\text{bot}}^3} / \overline{z_{\text{bot}}^2}^{3/2}$. For model DECORR we assume $\sigma_s = 2\sigma_{s_*}$. The figure demonstrates that increase β_c increases $\zeta_{z_{\text{bot}}}$ for both models.

In the rest of this article, we will use β_c as a measure of the influence of the boundary condition $z_{\text{bot}} \geq 0$ on the statistics of τ .

5. ν - A_c RELATIONS

In Sect. 2 we found that the Jeffery–Austin model of single-layer cloud statistics (or alternatively the models of Considine et al.¹¹ and Wood and Taylor¹³) could not account for the relatively large values of ν observed in Landsat and MWR data. A model extension was developed in Sect. 3.2 that incorporates the boundary condition $z_{\text{bot}} \geq 0$. In this section we determine the effect of this boundary condition, or equivalently the parameter β_c , on ν - A_c relations.

Plots of ν vs A_c are shown in Fig. 4 for $\beta_c \in \{0, 0.3, 0.6, 0.8\}$ and Gaussian P_s and P_{s_*} . Also shown is the MWR data from Fig. 2. The β_c -dependence of both models is similar; increasing β_c increases ν at fixed A_c . However model DECORR exhibits a relatively greater β_c -dependence than model NOZTOP. Overall, the effect of the boundary condition $z_{\text{bot}} \geq 0$ —evaluated in the simplified framework of the Jeffery–Austin model—is able to explain the relatively large values of ν exhibited by the data.

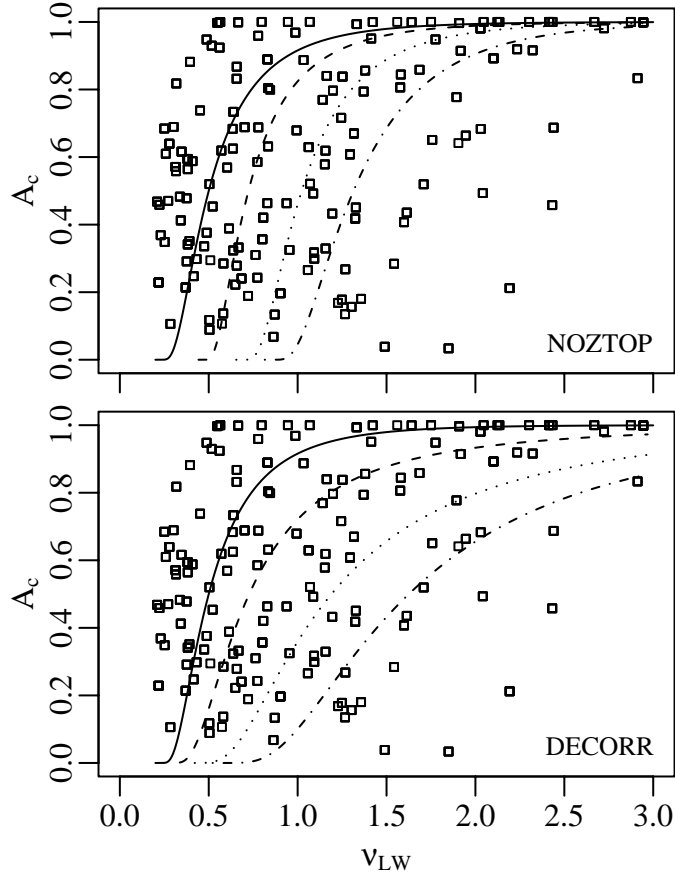


Figure 4. Plots of ν_{LW} vs A_c for model NOZTOP (upper panel) and DECORR (lower panel) with Gaussian P_s and P_{s^*} . The moments of τ_{LW} are calculated from Eq. (11) and A_c is given in Eqs. (13–14). Lines represent different β_c : 0 (—), 0.3 (–), 0.6 (– · –), and 0.8 (···). For model DECORR we assume $\sigma_s = 2\sigma_{s^*}$. The figures reveal that increasing β_c increases ν_{LW} at fixed A_c .

6. IMPACT OF β_c ON REFLECTIVITY

In this section we consider the impact of the boundary condition $z_{\text{bot}} \geq 0$, i.e. $\beta_c > 0$, on the mean in-cloud average SW reflectivity, \overline{R}_{SW} . We assume $R_{\text{SW}}(\tau)$ is given by the delta-Eddington 2-stream solution in the perfectly scattering limit²³, hemispherically averaged over solar zenith angle. For the present model:

$$\overline{R}_{\text{SW}} = A_c^{-1} \int \int R(\tau_{\text{SW}}(\xi, \xi_2)) P_{s^*}(\xi) d\xi P_s(\xi_2) d\xi_2,$$

where τ_{SW} is given by Eq. (12).

Our interest in this section is not the effect of β_c on the GCM diagnosis of grid-column averaged quantities, e.g. A_c and $\overline{\tau}$. Rather we are interested in the effect of β_c on P_τ at fixed $\overline{\tau}$ and $\overline{\tau^2}$, equivalently at fixed $(\overline{\tau}, \nu)$. Thus we assume that $(\overline{\tau}, \nu)$ are given and it is our task to determine \overline{R} .

Our first result is that $P_\tau(\tau = \xi | \overline{\tau}, \nu)$ is approximately independent of β_c for model DECORR and Gaussian P_{s^*} and P_s (not shown). Thus although β_c effects the diagnosis of $(\overline{\tau}, \nu)$, it does not effect the shape of P_τ at fixed $(\overline{\tau}, \nu)$. Turning our attention to model NOZTOP we find that, in this case, $P_\tau(\tau = \xi | \overline{\tau}, \nu)$ does have a

discernible β_c -dependence. The β_c -dependence of P_τ impacts \bar{R} . This is shown in Fig. 5 where \bar{R}_{SW} calculated for NOZTOP, $\bar{\tau} \in \{3, 10, 30\}$ and $\nu \in \{5/3, 3\}$ is plotted as a function of β_c for $0 \leq \beta_c \leq 0.8$ (lines) and Gaussian P_s . Also shown is the PPH approximation $\bar{R}_{\text{PPH}} = R(\bar{\tau}_{\text{SW}})$ (symbols), corresponding to $\nu \rightarrow \infty$. All reflectivities are normalized by $\bar{R}_{\text{SW}}(\beta_c = 0)$.

We note first the well-established result that \bar{R}_{PPH} overestimates \bar{R} . This overestimation is the range 10–15% at $\nu = 5/3$ (upper-panel) and 6–8% at $\nu = 3$ (lower-panel). Second we find that increasing β_c decreases \bar{R} for model NOZTOP. This decrease is in the range 0–4% at $\nu = 5/3$ and 0–3% at $\nu = 3$. Furthermore the relative decrease in \bar{R} increases as $\bar{\tau}$ increases. Thus we conclude the boundary condition $z_{\text{bot}} \geq 0$ damps \bar{R} at fixed $(\bar{\tau}, \nu)$ thereby increasing the relative error associated with the PPH approximation. Since \bar{R} is β_c -independent for model DECORR we further conclude that the correlation $\langle s_* s \rangle$ plays a crucial role in determining the net effect of the boundary-condition $z_{\text{bot}} \geq 0$ on \bar{R} .

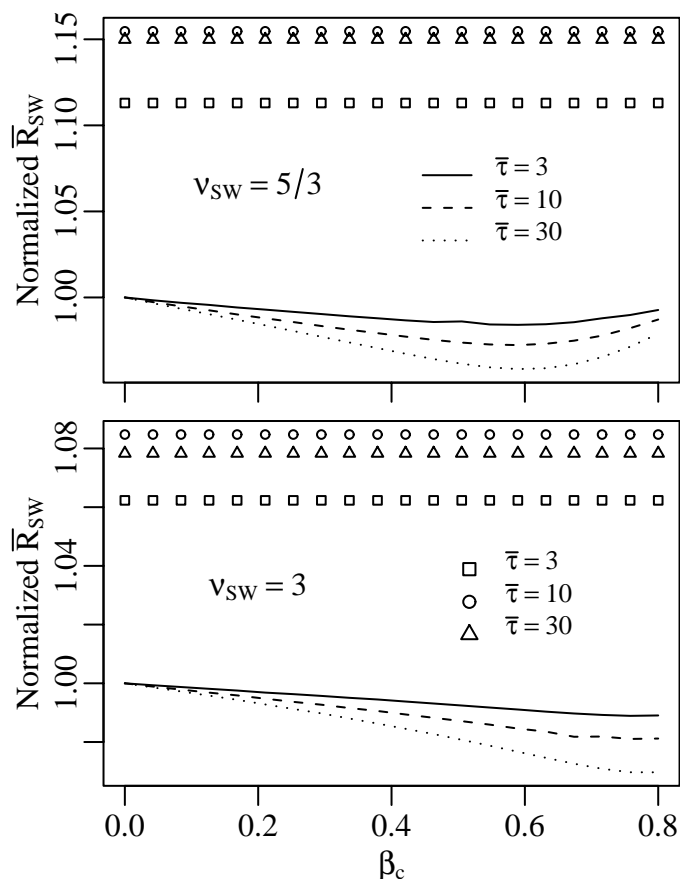


Figure 5. Plots of \bar{R} vs β_c for model NOZTOP, $\bar{\tau} \in \{3, 10, 30\}$ and $\nu = 5/3$ (upper-panel) and $\nu = 3$ (lower-panel). Lines are $\bar{R}_{\text{SW}}(\beta_c)$ calculated from Eq. (12), Gaussian P_s and $R(\tau)$ from Eq. 24 in Meador and Weaver²³. Symbols are the PPH-approximation $\bar{R}_{\text{PPH}} = R(\bar{\tau}_{\text{SW}})$, corresponding to $\nu \rightarrow \infty$. All reflectivities are normalized by $\bar{R}_{\text{SW}}(\beta_c = 0)$.

7. SUMMARY

Recently developed models of low-cloud statistical properties relate A_c and the moments of τ to underlying stochastic distributions: Considine et al.¹¹ specify a Gaussian distribution of cloud-thickness, Wood and

Taylor¹³ begin with conserved variables (θ, q_t) and Jeffery and Austin¹⁴ use (θ, q_t) and, in addition, include cloud-top height fluctuations, z'_{top} . In the work of Considine et al.¹¹ and Jeffery and Austin¹⁴ discussed above z_{bot} -skewness, $\zeta_{z_{\text{bot}}}$, is not explicitly considered while in the Wood and Taylor¹³ model, $\zeta_{z_{\text{bot}}} \leq 0$. In contrast, in-situ and surface-based measurements of z_{bot} distributions of low-clouds often indicate a positive skewness^{15–17}.

In this work we postulate the existence of a large-scale minimum lifting condensation level and we suggest that this thermodynamic boundary breaks the translational invariance assumed in recent models, leading to $\zeta_{z_{\text{bot}}} > 0$ under conditions of high boundary-layer relative humidity, RH. To test our hypothesis we explicitly incorporate the constraint $z_{\text{bot}} \geq 0$ into the Jeffery-Austin model of low-cloud optical variability where the reference height $z = 0$ is a large-scale minimum lifting condensation level. A parameter β_c is introduced that represents the relative occurrence of cloud liquid water at $z = 0$ and, thereby, the influence of the constraint $z_{\text{bot}} \geq 0$. We find, indeed, that $\zeta_{z_{\text{bot}}}$ increases with increasing β_c .

A model analysis reveals that the dimensionless parameter $\nu = (\bar{\tau}/\sigma_\tau)^2$ introduced by Barker et al.⁷ increases with increasing β_c at fixed A_c . This behaviour is significant because both Landsat scenes⁷ and ARM MWR time series exhibit relatively large values of ν that are not explained by the Jeffery-Austin model at $\beta_c = 0$. However, the 24-hour MWR data segments also contain a diurnal signal which may influence ν at a given A_c . In the future we hope to incorporate a diurnal-cycle into our statistical approach.

A preliminary analysis of the impact of β_c , i.e. the influence of $z_{\text{bot}} \geq 0$, on mean in-cloud SW reflectivity, \bar{R} , reveals that increasing β_c decreases \bar{R} at fixed $(\bar{\tau}, \nu)$ when $z'_{\text{bot}} = 0$ —the special case considered by Wood and Taylor¹³. This decrease is in the range 0–4% for $\beta_c \leq 0.8$ and increases with increasing $\bar{\tau}$; the further reduction in cloud albedo enhances the well-known PPH bias that results from $\nu < \infty$. On the other hand, when cloud-top height fluctuations are large and strongly correlated with z'_{bot} then \bar{R} is approximately β_c -independent at fixed $(\bar{\tau}, \nu)$. These results suggest that the influence of the boundary condition $z_{\text{bot}} \geq 0$ on low-cloud SW feedback is strongly modulated by the joint $z_{\text{bot}}-z_{\text{top}}$ statistics.

ACKNOWLEDGMENTS

Data were obtained from the Atmospheric Radiation Measurement (ARM) Program sponsored by the U.S. Department of Energy, Office of Science, Office of Biological and Environmental Research, Environmental Sciences Division. AD thanks the ARM Program for partial financial support. We thank Nicole Jeffery for a reading of this article.

REFERENCES

1. Harshvardhan and D. A. Randall. Comments on "The parameterization of radiation for numerical weather prediction and climate models". *Mon. Wea. Rev.*, 113:1832–1833, 1985.
2. G. L. Stephens. Radiative transfer through randomly fluctuating optical media. Part I. *J. Atmos. Sci.*, 45:1818–1836, 1988.
3. G. L. Stephens. Radiative transfer through randomly fluctuating optical media. Part II. *J. Atmos. Sci.*, 45:1837–1848, 1988.
4. R. F. Cahalan, W. Ridgway, W. J. Wiscombe, T. L. Bell, and J. B. Snider. The albedo of fractal stratocumulus clouds. *J. Atmos. Sci.*, 51(16):2434–2455, 1994.
5. Z. N. Kogan, D. K. Lilly, Y. L. Kogan, and V. Filyushkin. Evaluation of radiative parameterizations using an explicit cloud microphysical model. *Atmos. Res.*, 35:157–172, 1995.
6. H. W. Barker and B. A. Wielicki. Parameterizing grid-averaged longwave fluxes for inhomogeneous marine boundary layer clouds. *J. Atmos. Sci.*, 54(24):2785–2798, 1997.
7. H. W. Barker, B. A. Wielicki, and L. Parker. A parameterization for computing grid-averaged solar fluxes for inhomogeneous marine boundary layer clouds. Part II: Validation using satellite data. *J. Atmos. Sci.*, 53(16):2304–2316, 1996.

8. L. Oreopoulos and R. Davies. Plane parallel albedo biases from satellite observations. Part I: Dependence on resolution and other factors. *J. Climate*, 11:919–932, 1998.
9. L. Oreopoulos and R. Davies. Plane parallel albedo biases from satellite observations. Part II: Parameterizations for bias removal. *J. Climate*, 11:933–944, 1998.
10. R. Pincus, S. A. McFarlane, and S. A. Klein. Albedo bias and the horizontal variability of clouds in subtropical marine boundary layers: Observations from ships and satellites. *J. Geophys. Res.*, 104(D6): 6183–6191, 1999.
11. G. Considine, J. A. Curry, and B. Wielicki. Modeling cloud fraction and horizontal variability in marine boundary layer clouds. *J. Geophys. Res.*, 102(D12):13517–13525, 1997.
12. R. Pincus and S. A. Klein. Unresolved spatial variability and microphysical process rates in large-scale models. *J. Geophys. Res.*, 105(D22):27059–27065, 2000.
13. R. Wood and J. P. Taylor. Liquid water path variability in unbroken marine stratocumulus cloud. *Q. J. R. Meteorol. Soc.*, 127:2635–2662, 2001.
14. C. A. Jeffery and P. H. Austin. Unified treatment of the thermodynamic and optical variability of unresolved low clouds. *J. Atmos. Sci.*, 2002. To appear.
15. C. W. Fairall, J. E. Hare, and J. B. Snider. An eight-month sample of marine stratocumulus cloud fraction, albedo, and integrated liquid water. *J. Climate*, 3:847–864, 1990.
16. K. D. Poore, J. Wang, and W. B. Rossow. Cloud layer thickness from a combination of surface and upper-air observations. *J. Climate*, 8:550–568, 1995.
17. J. Wang, W. B. Rossow, T. Uttal, and M. Rozendaal. Variability of cloud vertical structure during ASTEX observed from a combination of rawinsonde, radar, ceilometer and satellite. *Mon. Wea. Rev.*, 127:2484–2502, 1999.
18. G. Sommeria and J. W. Deardorff. Subgrid-scale condensation in models of nonprecipitating clouds. *J. Atmos. Sci.*, 34:344–355, 1977.
19. G. L. Mellor. The Gaussian cloud model relations. *J. Atmos. Sci.*, 34:356–358, 1977. See also CORRIGENDA, **34**, 1483.
20. P. Bougeault. Modeling the trade-wind cumulus boundary layer. Part I: Testing the ensemble cloud relations against numerical data. *J. Atmos. Sci.*, 38:2414–2428, 1981.
21. C. Pontikis. Parameterization of the cloud optical thickness: Influence of clear air entrainment. *Geophys. Res. Lett.*, 20(23):2655–2658, 1993.
22. S. A. Klein, D. L. Hartmann, and J. R. Norris. On the relationships among low-cloud structure, sea surface temperature and atmospheric circulation in the summertime northeast Pacific. *J. Climate*, 8:1140–1155, 1995.
23. W. E. Meador and W. R. Weaver. Two-stream approximations to radiative transfer in planetary atmospheres: A unified description of existing methods and a new improvement. *J. Atmos. Sci.*, 37(3):630–643, 1980.